ACS APPLIED MATERIALS & INTERFACES

Research Article

www.acsami.org

UV-Light-Induced Improvement of Fluorescence Quantum Yield of DNA-Templated Gold Nanoclusters: Application to Ratiometric Fluorescent Sensing of Nucleic Acids

Zong-Yu Li,[†] Yun-Tse Wu,[†] and Wei-Lung Tseng*[,†,‡]

[†]Department of Chemistry, National Sun Yat-sen University, 70 Lien-hai Road, Kaohsiung 804, Taiwan

[‡]School of Pharmacy, College of Pharmacy, Kaohsiung Medical University, Kaohsiung 807, Taiwan

Supporting Information

ABSTRACT: The use of DNA as a template has been demonstrated as an effective method for synthesizing different-sized silver nanoclusters. Although DNA-templated silver nanoclusters show outstanding performance as fluorescent probes for chemical sensing and cellular imaging, the synthesis of DNA-stabilized gold nanoclusters (AuNCs) with high fluorescence intensity remains a challenge. Here a facile, reproducible, scalable, $NaBH_4$-free, UV-light-assisted method was developed to prepare AuNCs using repeats of 30 adenosine nucleotides (A_{30}). The maximal fluorescence of A_{30}-stabilized AuNCs appeared at 475 nm with moderate quantum yield, two fluorescence lifetimes, and a small amount of Au^+ on the surface of the Au core. Results of size-exclusion chromatography revealed that A_{30}-stabilized AuNCs were more compact than A_{30}. A series of control experiments showed that UV light played a dual role in the reduction of gold-ion precursors and the decomposition of citrate ions. A_{30} also acted as a stabilizer to prevent the aggregation of AuNCs. In addition, single-stranded DNA (ssDNA) consisting of an AuNC-nucleation sequence and a hybridization sequence was utilized to develop a AuNC-based ratiometric fluorescent probe in the presence of the double-strand-chelating dye SYBR Green I (SG). Under conditions of single-wavelength excitation, the combination of AuNC/SG-bearing ssDNA and perfectly matched DNA emitted fluorescence at 475 and 525 nm, respectively. The formed AuNC/SG-bearing ssDNA enabled the sensitive, selective, and ratiometric detection of specific nucleic acid targets. Finally, the AuNC-based ratiometric probes were successfully applied to determine specific nucleic acid targets in human serum.

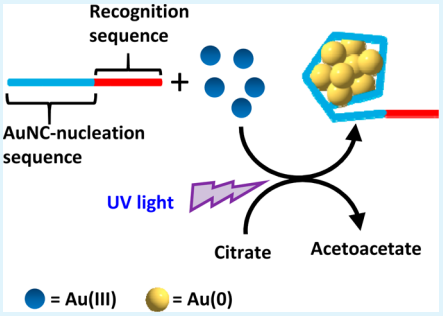

KEYWORDS: *gold nanoclusters, DNA, UV light, fluorescence, ratiometric sensor*

INTRODUCTION

Gold-based nanomaterials have received substantial attention in the past decade because of their intriguing size- and shape-dependent optical, electrical, and catalytic properties.[1,2] Of these properties, the optics of gold-based nanomaterials are perhaps most interesting; gold-based nanomaterials that are larger than 3 nm possess size- and shape-dependent surface plasmon resonance (SPR) caused by the interaction of light with electrons on the gold surface. At the resonance wavelength, SPR can generate strong light scattering, a local electromagnetic field, and localized heat release.[1] As the size of gold-based nanomaterials approaches the Fermi wavelength of an electron, they become ultrasmall "gold nanoclusters" (AuNCs) that exhibit moleculelike properties such as strong fluorescence[3] and quantized charging.[4,5] In addition to being ultrasmall, AuNCs are biocompatible and photostable. These properties enable AuNCs to serve as fluorescent probes for use in chemosensing, molecular imaging, and biolabeling.[6−8] Although silver nanoclusters have similar advantages to AuNCs, their fluorescence is sensitive to the concentration of chloride anions because of strong complexation between Ag(I) and chloride anions.[9] In addition, silver-based nanomaterials are susceptible to oxidizing agents.[10]

Numerous innovative synthesis methods have been developed for preparing differently sized AuNCs with fluorescent emissions from the UV to the near-IR regions. Ligand-induced removal of gold atoms from the surface of nanometer-sized gold particles (>2 nm) results in the formation of fluorescent AuNCs via electron injection from the ligands to the gold particles.[11,12] Long-chain thiols such as 11-mercaptoundecanoic acid,[13] dihydrolipoic acid,[14] 11-mercapto-3,6,9-trioxaundecyl-α-D-mannopyranoside,[15] and glutathione[16] are most commonly used as etching ligands for producing highly fluorescent AuNCs. Choosing a suitable capping ligand and template is an alternative method for producing fluorescent AuNCs. For example, near-IR-emitting AuNCs with a quantum yield (QY) of 2.9% were prepared via $NaBH_4$ reduction of a gold precursor in the presence of lipoic acid,[17,18] whereas blue-emitting AuNCs with a QY of 8.3% were synthesized by reducing a

Received: August 20, 2015
Accepted: October 7, 2015
Published: October 7, 2015

DOI: 10.1021/acsami.5b07766
ACS Appl. Mater. Interfaces 2015, 7, 23708−23716

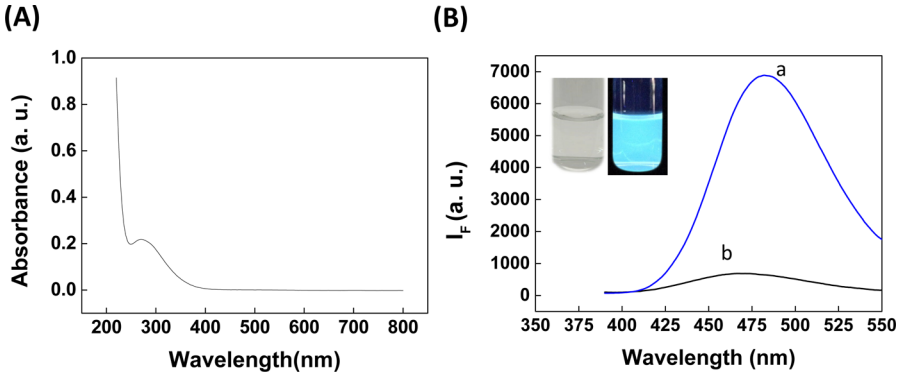

Figure 1. (A) Absorption spectrum of A_{30}-stabilized AuNCs. (B) Fluorescence spectra of A_{30}-stabilized AuNCs with (a) and without (b) the treatment of UV light. Inset: Digital photos of A_{30}-stabilized AuNCs under visible (left) and UV light (right).

mixture containing a gold precursor and 3-mercaptopropionic acid with $NaBH_4$.[19] Hydroxyl-terminated poly(amidoamine) dendrimer and bovine serum albumin have been utilized as templates for preparing blue-emitting Au_8 and red-emitting Au_{25} clusters, respectively.[20,21] Compared with thiols, proteins, and polymers, the use of DNA as a template for synthesis of fluorescent AuNCs in the presence of citrate[22] or dimethylamineborane[23] has been reported in relatively few studies. In addition, the application of DNA-templated AuNCs as a fluorescent probe lacks investigations because of low fluorescence intensity, although DNA molecules are widely used as recognition elements in nanomaterials for sensitive and selective detection of biomolecules and metal ions.

Photosynthetic methods are well-established for the preparation of gold-based nanomaterials in the presence of adenosine,[24] benzoin,[25] cationic surfactants,[26] CdS nanorods,[27] and carbon nanotubes.[28] Compared with standard chemical approaches, light-assisted synthesis of gold-based nanomaterials offers the following distinct advantages: (1) The process is simple and green. (2) The rate of reaction can be controlled by tuning the power density and the irradiation wavelength. (3) The reducing agent is uniformly distributed throughout the solution. Sodium citrate ions are commonly utilized as the reducing agent for the synthesis of metal nanoparticles,[29] and the major oxidized species of citrate ions during the synthesis has been identified as acetoacetate.[30] The decomposition of citrate to acetoacetate was also observed when citrate was irradiated with visible light in the presence of silver nanoparticles.[31,32] Without those thoughts in mind, in the present study, we proposed that UV light could be used to stimulate the decomposition of citrate ions. We identified the chemical roles of UV light, citrate, and polyadenosine in the UV-light-assisted synthesis of AuNCs. In addition, we used a combination of the double-strand-chelating dye SYBR Green (SG) and blue-emitting AuNCs to design a ratiometric fluorescent probe for specific nucleic acid targets.

RESULTS AND DISCUSSION

UV-Light-Assisted Formation of AuNCs. The synthesis of DNA-templated AuNCs was achieved by irradiating an aqueous gold-ion precursor solution with 305 nm UV light in the presence of 1 μM A_{30} and citrate ions at pH 6.0. This one-step reaction proceeded at ambient temperature for 24 h. The as-prepared solution exhibited a broad absorption band without a localized SPR band, which indicated the possible formation of AuNCs (Figure 1A). Upon excitation at 290 nm, the as-synthesized AuNCs emitted a maximal fluorescence at 475 nm (curve a in Figure 1B). Because polyadenosine-containing adenine exhibits fluorescence when excited at 290 nm, we compared the fluorescence spectra of A_{30} and A_{30}-stabilized AuNCs. Figure S1 shows that the emission at 475 nm resulted from A_{30}-stabilized AuNCs rather than A_{30}. To initiate a control experiment, the reaction of $HAuCl_4$, A_{30}, and citrate ions was allowed to proceed for 24 h without UV irradiation. The resulting product fluoresced weakly, which indicates that UV light is essential to convert gold-ion precursor to fluorescent products (curve b in Figure 1B).The emission at 475 nm that corresponds to A_{30}-stabilized AuNCs suggests that Au_8 clusters formed successfully in A_{30} via the simple relationship $E_{Fermi}/N^{1/3}$, which was predicted using the spherical Jellim model.[33] The emission wavelength is almost equal to that reported for lysozyme-stabilized (λ_{max} = 455 nm),[34] BSA-mediated (λ_{max} =450 nm),[35] polyethylenimine-encapsulated (λ_{max} = 455 nm),[36] and dendrimer-capped (λ_{max} = 458 nm) AuNCs.[37] Because the excitation wavelength varied from 280 to 370 nm, the maximal emission wavelength of A_{30}-stabilized AuNCs remained almost constant (Figure S2). This result clearly indicates that the band at 475 nm was indeed a fluorescence signal rather than scattering from AuNCs and A_{30}. The absolute QY of A_{30}-stabilized AuNCs with and without the treatment of UV light was determined to be 2.2 and 0.5%, respectively. Lifetime values of Au_8 clusters were obtained by numerically fitting the fluorescence at 475 nm (excitation at 390 nm). The blue-emitting Au_8 clusters exhibited two lifetimes of 3 ns (approximately 40%) and 40 ns (approximately 60%) (Figure S3). The short lifetime could be attributed to the singlet transition between the d band and sp band, whereas the long lifetime probably arose from triplet−singlet intraband transition. The identification of two lifetimes in the present study agrees with the findings of previous AuNC studies.[34−37] The stability of A_{30}-stabilized AuNCs was examined by monitoring their fluorescence under various conditions. When the pH of the solution varied from 3.0 to 11.0, the fluorescence intensity at 475 nm of A_{30}-stabilized AuNCs remained almost unchanged (Figure S4). In the presence of 200 mM NaCl, a 20% decrease in the fluorescence intensity of A_{30}-stabilized AuNCs was observed (Figure S5). In contrast, previous studies reported that the presence of 200 mM NaCl caused about 99% fluorescence quenching of DNA-templated silver nanoclusters.[38,39] A slight decrease in the fluorescence of A_{30}-stabilized AuNCs was observed after prolonged storage at 4 °C for 5 months (Figure S6). These results suggest that A_{30}-stabilized AuNCs have potential for use as molecular sensors under a

DOI: 10.1021/acsami.5b07766
ACS Appl. Mater. Interfaces 2015, 7, 23708−23716

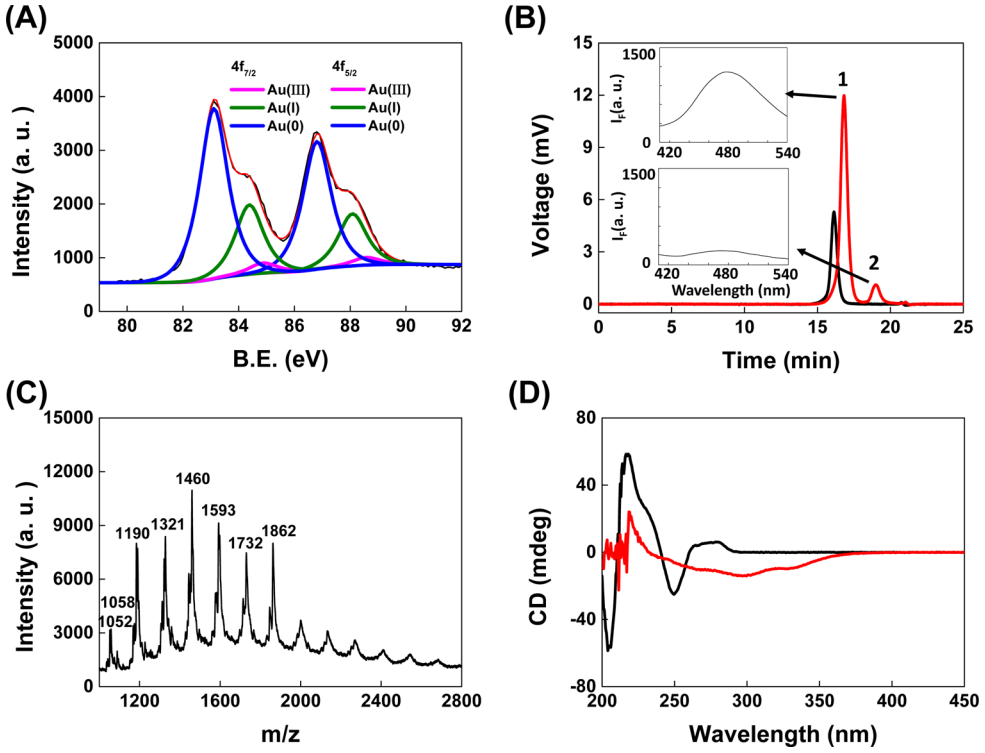

Figure 2. Characterization of A_{30}-stabilized AuNCs. (A) XPS spectrum of A_{30}-stabilized AuNCs. (B) SEC chromatograms of A_{30} (black line) and A_{30}-stabilized AuNCs (red line). Inset: Fluorescence spectra of peaks **1** and **2**. (C) Negative-ion MALDI-TOF mass spectrum of A_{30}-stabilized AuNCs. (D) CD spectra of A_{30} (black line) and A_{30}-stabilized AuNCs (red line).

variety of physiological conditions. With a reliable irradiation process by UV light, the synthesis method presented above had good batch-to-batch reproducibility (Figure S7). In addition, Figure S8 shows that the synthesis method can be scaled up to large volumes (e.g., 20 mL).

The valence states of A_{30}-stabilized AuNCs were determined from their X-ray photoelectron spectroscopy (XPS) spectra. Deconvolution of the Au $4f^{7/2}$ spectrum of A_{30}-stabilized AuNCs revealed the existence of Au^0, Au^+, and Au^{3+}. According to the best fit of the experimental data, A_{30}-stabilized AuNCs consisted of 4% Au^{3+}, 28% Au^+, and 68% Au^0 (Figure 2A). Apparently, UV light does indeed stimulate the conversion of $HAuCl_4$ to AuNCs in the presence of citrate ions and A_{30}. Size-exclusion chromatography (SEC) was used to confirm the formation of AuNCs because this separation method can distinguish solutes on the basis of their sizes. In contrast to the chromatogram of A_{30} (black line in Figure 2B), the chromatograms of A_{30}-stabilized AuNCs exhibited two resolved peaks (black line in Figure 2B). Because the molecular weight of A_{30} resembles that of A_{30}-stabilized Au_8 clusters, we proposed that they would have similar retention times. Accordingly, a large peak, peak **1**, with a retention time at 16.8 min, was collected manually from the SEC column and analyzed by fluorescence spectroscopy. A small peak, peak **2**, with a retention time at 18.9 min, was also collected for further analysis. The fluorescence and absorption spectra of peak **1** was almost the same as that of an A_{30}-stabilized-AuNC solution (inset in Figure 2B; also Figure S9); thus, peak **1** corresponded to the A_{30}-stabilized AuNCs. Peak **2** did not exhibit fluorescence in the spectral region of interest (inset in Figure 2B), which implies that it did not contain AuNCs. This result suggests that the presence of the byproduct in an A_{30}-stabilized-AuNC solution did not interfere with their optical properties. Although A_{30}-stabilized AuNCs have a larger molecular weight than A_{30}, they were eluted later. This could be because AuNCs contact the DNA strand through nucleobase coordination, which results in a condensed and compact structure. Similarly, Obliosca et al.[40] used SEC to determine the size of DNA-stabilized silver nanoclusters; they revealed that the retention time of these nanoclusters was slightly slower than that of DNA strands. We also measured the hydrodynamic radius of A_{30}-stabilized AuNCs to determine the impact of AuNC adducts on DNA shape. SEC analysis of five single-stranded polyadenosines (A_{10}, A_{20}, A_{30}, A_{40}, and A_{50}) resulted in a calibration curve describing the retention time according to the logarithm of the hydrodynamic radius (Figure S10). Importantly, the hydrodynamic radii of these polyadenosines progressively increased as their length increased. The hydrodynamic size of A_{30}-stabilized AuNCs was 42% smaller than that of A_{30}.

In addition to the XPS and SEC measurements, the results of matrix-assisted laser desorption/ionization time-of-flight mass spectrometry (MALDI-TOF-MS) provided strong supporting evidence for the successful formation of AuNCs. In MALDI-TOF-MS analysis of A_{30} and A_{30}-stabilized AuNCs, 3,4-diaminobenzophenone was chosen as the matrix because it provides a low detection limit, high resolution, and less fragmentation.[41] In contrast to the mass spectra of 3,4-diaminobenzophenone (Figure S11), the mass spectra of A_{30} and A_{30}-stabilized AuNCs consisted of a broad range of peaks in the higher mass range (Figures S12 and 2C). Apparently, the peaks between m/z 1200 and 2800 originated from A_{30} and A_{30}-stabilized AuNCs rather than 3,4-diaminobenzophenone. The mass spectrum of A_{30}-stabilized AuNCs consisted of major peaks at m/z 1052, 1058, 1190, 1321, 1460, 1593, 1732, and 1862, which corresponded to $[6Au + Na + A_{30}]^{-10}$, $[6Au + 3Na + A_{30}]^{-10}$, $[7Au + A_{30}]^{-9}$, $[6Au + 2Na + A_{30}]^{-8}$, [4Au + 4 Na +

DOI: 10.1021/acsami.5b07766
ACS Appl. Mater. Interfaces 2015, 7, 23708−23716

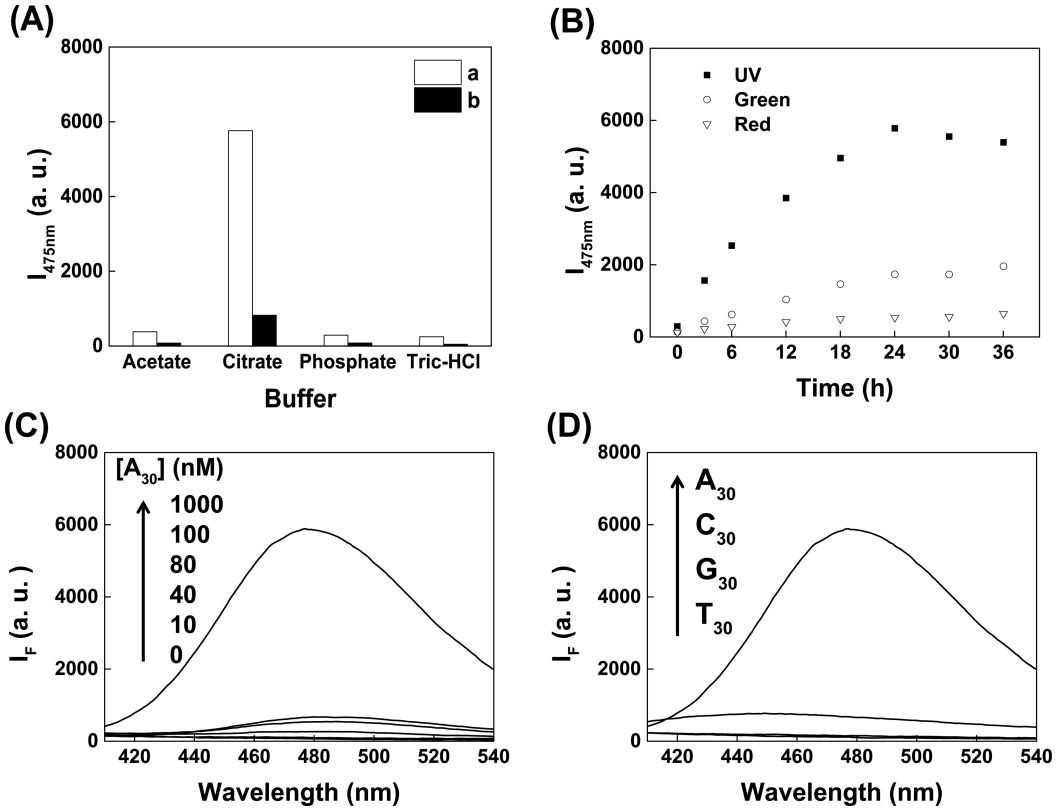

Figure 3. Effect of the parameters on the synthesis of A_{30}-stabilized AuNCs. (A) Fluorescence intensity at 475 nm of the product synthesized from different buffer solution with (a) and without UV irradiation (b). (B) Temporal change in fluorescence intensity at 475 nm of the precursor solution under the irradiation of UV-, green-, and red-emitting LEDs. (C and D) Effect of (C) the A_{30} concentration and (D) the DNA sequence on the fluorescence spectra of the product obtained from photoreaction of UV light and the precursor solution. (A–D) The precursor solution contains (A) 50 μM $HAuCl_4$, 1 μM A_{30}, and 5 mM buffer solution, (B) 50 μM $HAuCl_4$, 1 μM A_{30}, and 5 mM sodium citrate, (C) 50 μM $HAuCl_4$, 0–1000 nM A_{30}, and 5 mM sodium citrate, and (D) 50 μM $HAuCl_4$, 1 μM oligonucleotide, and 5 mM sodium citrate.

$A_{30}]^{-7}$, $[Au + Na + A_{30}]^{-6}$, $[5Au + 3Na + A_{30}]^{-6}$, and $[9Au + 3Na + A_{30}]^{-6}$, respectively. The formation of sodium adducts was generally observed in negative-mode MALDI-TOF-MS.[41,42] This result indicates that A_{30} can complex with AuNCs. In addition, the number of Au atoms in A_{30}-stabilized AuNCs was less than nine; thus, their emission wavelength could be located between 400 and 500 nm. Transmission electron microscopy (TEM) imaging reveals that the majority of as-synthesized AuNCs were smaller than 2 nm in size (Figure S13). These findings are consistent with the aforementioned results from the fluorescence spectroscopy and SEC analyses.

Circular dichroism (CD) spectroscopy analyses provided another line of evidence for the strong interaction between polyadenosine and AuNCs. Compared with the CD spectrum of A_{30}, A_{30}-stabilized AuNCs exhibited a remarkable change in ellipticity at the region from 200 to 350 nm, which suggests that the presence of AuNCs triggers a dramatic change in the conformation of A_{30} (Figure 2D). This finding is in agreement with a specific result from SEC analysis that showed A_{30}-stabilized AuNCs had a shorter retention time than A_{30}.

Chemical Role of Citrate Ions and UV Light. To determine the role of citrate ions in the UV-light-assisted synthesis of AuNCs, four different buffer systems (sodium acetate, sodium phosphate, Tris-HCl, and sodium citrate) were incubated with a solution containing $HAuCl_4$ and A_{30} for 24 h at pH 6.0. Without UV light irradiation, weak fluorescence was only observable where the solution was buffered with sodium citrate (Figure 3A). Compared with the other buffer systems, citrate ions were still capable of reducing $HAuCl_4$ to AuNCs in the presence of A_{30} without UV light irradiation. This result is consistent with the observation that citrate ions were effective to reduce $HAuCl_4$ to AuNCs in the presence of repeats of 5 adenosine nucleotides.[43] When a mixture of $HAuCl_4$, A_{30}, and citrate ions was irradiated with UV light, the generated products emitted strong fluorescence at 475 nm. Thus, UV-light-induced decomposition of citrate ions apparently supplies the electrons that facilitate the conversion of $HAuCl_4$ to AuNCs. To confirm this result, the synthesis of A_{30}-stabilized AuNCs proceeded at 90 °C without UV light irradiation. Figure S14 shows that the fluorescence spectrum of the products obtained from UV-light-assisted synthesis resembled that of the products synthesized from heating-assisted synthesis. This result clearly suggests that the heating method intensified the oxidation of citrate to acetoacetate supplying the electrons for the reduction of $HAuCl_4$ which is consistent with the previous finding.[30] Therefore, the oxidation of citrate ions was determined to be a major factor governing the synthesis of DNA-templated AuNCs.

The absorption and fluorescence spectra of A_{30}-stabilized AuNCs were monitored at different growth stages under conditions of UV light irradiation. Prior to irradiation, a mixture of $HAuCl_4$, citrate, and A_{30} had a strong absorbance band centered at 260 nm, which can be attributed to the intrinsic absorbance of A_{30} (Figure S15).[44] When the precursor solution was irradiated with UV light, the absorbance intensity

DOI: 10.1021/acsami.5b07766
ACS Appl. Mater. Interfaces 2015, 7, 23708–23716

progressively increased with time from 300 to 400 nm (Figure S15). Additionally, the fluorescence intensity of the precursor solution at 475 nm gradually increased with irradiation time (Figure 3B). The changes in absorbance and fluorescence spectra were attributed to the conversion of $HAuCl_4$ to AuNCs.

The effect of irradiation wavelength on the photoreduction process was also investigated to confirm the role of UV light in the synthesis of DNA-templated AuNCs. When the precursor solution was separately irradiated with green- and red-emitting LEDs, the obtained product exhibited weak absorbance in the range from 300 to 400 nm (Figure S16), accompanied by the presence of weak fluorescence intensity at 475 nm (Figure 3B). This indicates that UV light is more efficient for the formation of AuNCs than green or red light, which in turn implies that the decomposition of citrate ions proceeds relatively quickly when using UV light irradiation. However, this could also be explained by the stability of the $HAuCl_4$ complexes being relatively weak under conditions of UV illumination, which would lead to the dissociation of Au^{3+} from the complex.[45] Here, cyclic voltammetry (CV) was utilized to support the conversion of $HAuCl_4$ to AuNCs via UV light irradiation. CV analysis of the precursor solution generated one reduction wave at +0.28 V in the forward potential scan from +1.0 to −1.0 V and one oxidation wave at +0.95 V in the reverse potential scan (Figure S17A). The reduction wave results from the reduction of $AuCl_4^-$ to Au^0, whereas the oxidation wave is due to the oxidation of the formed Au^0.[46] After the photoreaction of UV light and the precursor solution had proceeded for 4 h, CV analysis of the obtained products revealed that the Au^{3+} reduction wave was shifted to +0.47 V and its current became smaller (Figure S17B). When the photoreaction continued to 24 h, the Au^{3+} reduction wave was no longer observed in the CV voltammogram of the obtained products (Figure S17C). The shift in the potential of the Au^{3+} reduction wave indicates that once AuNCs are formed a much lower potential is required for additional formation of AuNCs. Similarly, Chen and Huang[47] reported that the Au^{3+} reduction wave was shifted to an increased positive potential after the electrodeposition of Au nanoparticles on the electrode surface. The observed decrease in the current of the Au^{3+} reduction wave shows that the concentration of $HAuCl_4$ decreased with irradiation time. Importantly, the UV-light-assisted conversion of $HAuCl_4$ to AuNCs was complete after 24 h. In comparison, Lopez and Liu prepared adenosine-capped AuNCs with blue emission through a short time exposure of the adensoine−Au^{3+} complexes to UV light in the presence of citrate ions.[24] The difference in UV exposure time between the proposed and previous methods could be attributed to the fact that polyadensoine forms more stable complexes with Au^{3+} than adenosine. The reduction of the adenosine−Au^{3+} complexes is therefore much easier than that of the polyadenosine−Au^{3+} complexes.

Chemical Role of Polyadenosine. Short cytosine-rich DNA molecules have been used extensively as templates in the synthesis of silver nanoclusters because of the strong binding of cytosine to silver ions.[48] Because polyadenosine is capable of directly attaching to the surface of citrate-capped gold nanoparticles through the exocyclic amino group and ring nitrogen atoms,[49] we reasoned that the role of polyadenosine in the UV-light-assisted synthesis of AuNCs is to serve as a stabilizer. To confirm this hypothesis, preparation of AuNCs was carried out in the presence of different concentrations of A_{30}. After treating a mixture of citrate ions and $HAuCl_4$ with UV light in the absence of A_{30}, the obtained products exhibited an SPR band at 525 nm, which is the characteristic band of gold nanoparticles (Figure S18). Because of the absence of a stabilizer, the formed AuNCs were extremely unstable and aggregated to form large particles. As the concentration of A_{30} increased in the precursor solution, we observed a progressive decrease in the SPR band intensity (Figure S19), which was accompanied by a gradual increase in the fluorescence intensity (Figure 3C). These results indicate that increasing the A_{30} concentration facilitates the formation of AuNCs, and this can be attributed to A_{30} acting as a stabilizer to prevent the aggregation of AuNCs through aurophilic attraction. In other words, the attachment of polyadenosine on the surface of AuNCs inhibits their growth through electrostatic repulsion or steric hindrance. When A_{30} was replaced by 30-repeat thymines (T_{30}), cytosines (C_{30}), or guanines (G_{30}), UV-light-assisted synthesis of AuNCs was unsuccessful under identical conditions (Figure 3D). Therefore, in contrast to thymine, cytosine, and guanine, polyadenosine has a high affinity for AuNCs and is apparently able to prevent their aggregation in an aqueous solution.

On the basis of our experimental results and earlier studies, we concluded that five processes occurred during UV-light-assisted synthesis of AuNCs (Figure 4): (1) The interaction

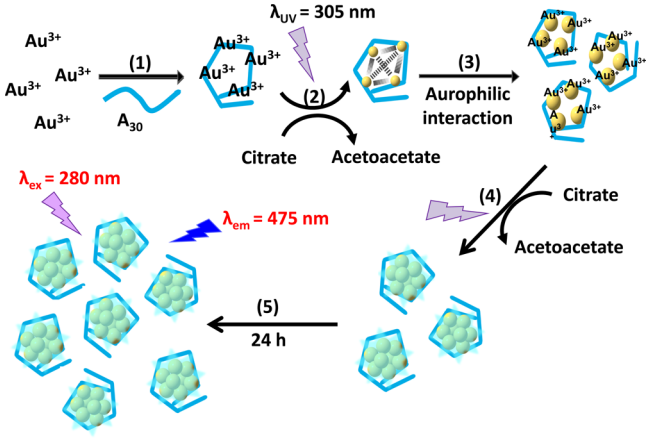

Figure 4. Step-by-step illustration of the procedure for UV-light-mediated synthesis of A_{30}-stabilized AuNCs in the presence of sodium citrate.

between Au^{3+} and adenine bases resulted in the formation of the Au^{3+}−polyadenosine complexes. (2) UV light induced the oxidation of citrate ions to acetoacetate and the produced electron converted gold ions to atomic Au^0. (3) The formed Au^0 tended to aggregate through aurophilic attraction.[50] (4) The electrons produced from oxidized citrate ions reduced gold ions on the surface of the assembled Au^0, thereby promoting a progressive increase in particle size; polyadenosine molecules acting as stabilizers attached to the surface of the formed AuNCs, preventing nanoclusters from coalescing with neighboring clusters. (5) The formation of A_{30}-stabilized AuNCs increased with increasing irradiation time and reached saturation after 24 h.

Ratiometric Fluorescent Probes. Various factors, including environmental conditions, probe concentration, photobleaching, and stability of the light source, could interfere with the signal from the fluorescent sensor, which would result in inaccurate quantification. Theoretically, these shortcomings could be overcome by using a ratiometric fluorescent probe

DOI: 10.1021/acsami.5b07766
ACS Appl. Mater. Interfaces 2015, 7, 23708−23716

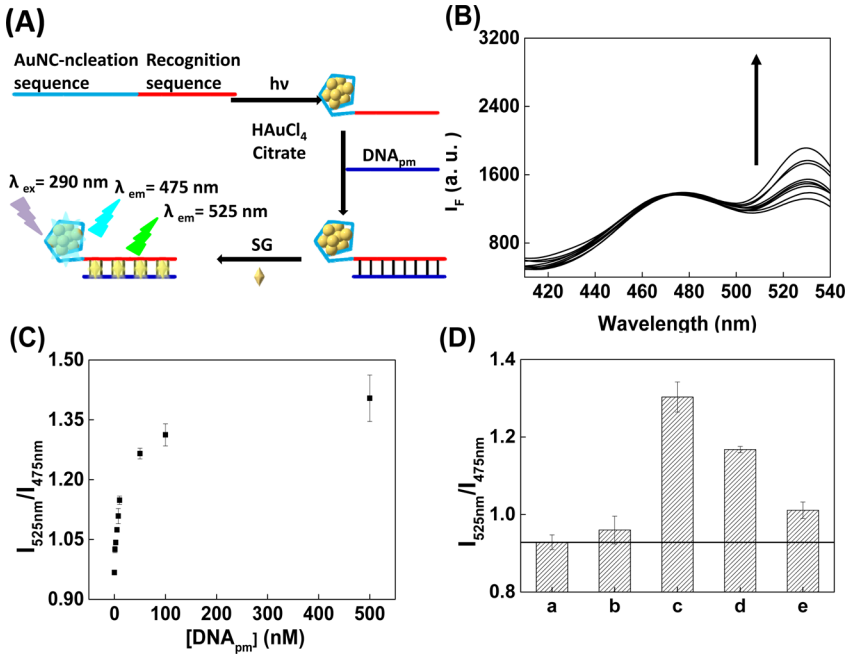

Figure 5. (A) Ratiometric detection of specific nucleic acid target via the combination of SG- and AuNC-bearing ssDNA. (B) Fluorescence spectra of AuNC/SG-bearing ssDNA in the presence of increasing DNA_{pm} concentration. The arrow indicates the signal changes with increasing the concentration of analyte: 0. 1. 2.5, 5, 7.5, 10, 50, 100, and 500 nM. (C) Plot of the I_{525nm}/I_{475nm} value versus theDNA_{pm} concentration. (D) I_{525nm}/I_{475nm} value of AuNC/SG-bearing ssDNA in (a) the absence and (b−e) presence of 10 nM (b) nontarget DNA, (c) DNA_{pm}, (d) single-base-mismatched DNA, and (e) double-base-mismatched DNA. The error bars represent standard deviations based on three independent measurements. The incubation time was 30 min. A mixture of 100 nM SG and 0.1× AuNC-bearing ssDNA was prepared in 10 mM Tris-HCl at pH 7.0.

because it offers built-in correction of the aforementioned factors.[51] To produce a probe such as this, single-stranded DNA (ssDNA) consisting of an AuNC-nucleation sequence (A_{30}) and a 22-base hybridization sequence was utilized as a template for the synthesis of AuNCs under the same conditions used during the synthesis of A_{30}-stabilized AuNCs (Figure 5A). Figure S20 shows that the emission band of the as-synthesized AuNCs was centered at approximately 475 nm, which resembled the emission wavelength of A_{30}-stabilized AuNCs. A mixture of SG (100 nM) and perfectly matched DNA (DNA_{pm}) was added to the AuNC-bearing ssDNA, and the resultant formation of double-stranded DNA (dsDNA) in the hybridization sequence interacted with the SG molecules to cause an increase in their fluorescence intensity at 525 nm (with an excitation of 290 nm; Figure S21). A concentration of 100 nM SG was chosen for this sensing system because a higher concentration of SG caused a higher fluorescence background and reduced the sensitivity of the proposed probe. In a control experiment, the addition of either perfectly matched DNA or SG to a solution of AuNC-bearing ssDNA did not affect the fluorescence of AuNCs (Figure S21). Additionally, the fluorescence intensities at 475 and 525 nm of AuNC/SG-bearing dsDNA, respectively, were similar to those of AuNC-bearing ssDNA and SG-labeled dsDNA at the same concentrations (Figure S22). This demonstrates that fluorescence resonance energy transfer from AuNCs to SG rarely occurred. These results strongly suggest that AuNC/SG-bearing ssDNA is well-suited for ratiometric detection of specific nucleic acid targets (Figure 5A).

Figure 5B shows that the fluorescence intensity at 525 nm (I_{525nm}) of AuNC/SG-bearing ssDNA gradually increased with the concentration of DNA_{pm}; however, this was accompanied by unchanged fluorescence intensity at 475 nm (I_{475nm}). A linear relationship was observed between the I_{525nm}/I_{475nm} values and DNA_{pm} concentration (Figure 5C) from 1 to 10 nM (R^2 = 9974). With a signal-to-noise ratio of 3 for DNA_{pm}, the limit of detection (LOD) was estimated as 0.3 nM. The sensitivity of this probe for DNA_{pm} is comparable to that of a molecular beacon with two fluorescent dyes.[52,53] Figure 5D shows that the I_{525nm}/I_{475nm} value obtained from the analysis of DNA_{pm} was higher than that obtained from the analysis of single-base-mismatched DNA, double-base-mismatched DNA, and nontarget DNA; thus, AuNC/SG-bearing ssDNA exhibited high selectivity toward DNA_{pm}. The feasibility of AuNC-bearing ssDNA was next validated by quantifying DNA_{pm} in human plasma sample. After samples of human plasma were spiked with a series of concentrations of DNA_{pm}, the DNA_{pm}-spiked samples were treated with the PureLink Genomic DNA Mini Kit. Note that this kit is designed for direct and efficient extraction of DNA from complex biological matrices. The extracted samples were then detected by the proposed probe. As the spiked concentration of DNA_{pm} was increased, we observed a gradual increase in the fluorescence intensity at 525 nm and a rare change in the fluorescence intensity at 475 nm. Plotting the I_{525nm}/I_{475nm} value against the spiked concentration of DNA_{pm} produced a linear plot over the range of 1 to 10 nM (R^2 = 9956). This result clearly reveals that DNA_{pm} was successfully detected in plasma by using AuNC/SG-bearing ssDNA.

CONCLUSIONS

In this study, UV light was introduced as a tool for the synthesis of DNA-templated AuNCs in the presence of citrate ions. The formation of A_{30}-stabilized AuNCs was driven by the UV-light-triggered oxidation of citrate ions and polyadenosine-induced inhibition of nanocluster aggregation. A functional ssDNA

DOI: 10.1021/acsami.5b07766
ACS Appl. Mater. Interfaces 2015, 7, 23708−23716

probe, which consisted of A_{30}-stabilized AuNCs and a recognition sequence for hybridization, was hybridized with target DNA to form dsDNA; the result was enhanced fluorescence intensity of SG at 525 nm and a rare change in the fluorescence intensity of A_{30}-stabilized AuNCs at 475 nm. The combination of SG, AuNC-bearing ssDNA, and DNA_{pm} resulted in the generation of AuNC/SG-bearing dsDNA, which emitted fluorescence at 475 and 525 nm under conditions of single-wavelength excitation. The sensing platform described here exhibited high sensitivity and high reproducibility, and it was able to discriminate between DNA_{pm} and single-base-mismatched DNA. To the best of our knowledge, this is the first example of the synthesis of DNA-templated AuNCs for sensitive and selective detection of specific nucleic acid targets. Because the fluorescence features of DNA-templated silver nanoclusters strongly rely on their DNA sequence,[54] we believe that different sizes of DNA-templated AuNCs could be synthesized by tuning the DNA sequence. Moreover, the availability of other DNA-binding fluorescent dyes as well as the sequence- and structure-dependent selectivity of DNA molecules such as aptamers will pave the way for the design and development of additional AuNC-based ratiometric fluorescence probes.

EXPERIMENTAL SECTION

Chemicals. Hydrogen tetrachloroaurate (III) dehydrate was purchased from Alfa-Aesar (Ward Hill, MD, USA). Bovine serum albumin (from bovine serum), NaOH, HCl, NaCl, Na_2HPO_4, NaH_2PO_4, H_3PO_4, Na_3PO_4, homocysteine, quinine sulfide, citric acid, trisodium citrate, tris(hydroxymethyl)aminomethane (Tris), acetic acid, sodium acetate, 3,4-diaminobenzophenone, AChE (EC1.1.3.7 from *Electrophorus electricus*, 1000 U mg^{-1}), ATC, bovine serum albumin, cytochrome C (from bovine heart), hemoglobin (from human erythrocytes), myoglobin (from equine heart), thrombin (from bovine serum), human serum albumin, and metal ions were ordered from Sigma-Aldrich (St. Louis, MO, USA). Lysozyme (from chicken egg white) and trypsin (from bovine pancreas) were obtained from MP Biomedicals (Irvine, CA). All DNA samples were synthesized from Neogene Biomedicals Corporation (Taipei, Taiwan). SG (10 000× ; 19.2 mM) was purchased from Molecular Probe, Inc. (Portland, OR); the molar absorption coefficient of SG at the optical wavelength of 494 nm is approximately 73 000 M^{-1} cm^{-1}. Milli-Q ultrapure water (Milli-Pore, Hamburg, Germany) was used in all of the experiments.

Instrumentation. The absorption and fluorescence spectra were recorded using a double-beam UV−vis spectrophotometer (Cintra 10e; GBC, Victoria, Australia) and a Hitachi F-7000 fluorometer (Hitachi, Tokyo, Japan), respectively. CV was conducted using a CHI 611c electrochemical analyzer (CHinstrument Inc., USA). A disposable electrochemical screen-printed electrode consisting of a carbon working electrode, a carbon counter electrode, and a Ag/AgCl reference electrode was purchased from Zensor R&D (Taichung, Taiwan). Time-resolved fluorescence measurements of A_{30}-stabilized AuNCs were carried out using a time-correlated single-photon counting system (Time-Harp 200, PicoQuant GmbH, Berlin, Germany) equipped with a pulsed diode laser at 390 nm (tens of ps pulse-width). The elemental compositions of A_{30}-stabilized AuNCs were measured by JAMP-9500F Auger Electron Spectroscopy (JEOL, Japan). CD was carried out on a JASCO modelJ-815 CD spectropolarimeter (JASCO, Corporation, Tokyo, Japan). The size-exclusion chromatography system consisted of a Spectra Series P100 isocratic pump (Thermo Separation Products, Waltham, MA, USA), a manual injector, a separation column (OHpak SB-804 HQ, Showa Denko America, Inc. New York, USA; 8.0 mm ID × 300 mm), and a Spectra Series UV100 detector (Thermo Separation Products, Waltham, MA, USA). TEM (JEM-1400, JEOL, Tokyo, Japan) was used to measure the size of A_{30}-stabilized AuNCs. MALDI-TOF MS (BrukerDaltonics, Germany) was carried out to determine the molecular weight of A_{30}-stabilized AuNCs. Prior to MALDI-TOF MS measurement, 3,4-diaminobenzophenone (0.01 g) was dissolved into a solution (1 mL) containing 70% acetonitrile and 0.1% trifluoroacetic acid. We mixed the as-prepared solution with an equal volume of the purified A_{30}-stabilized AuNCs and pipetted the resulting mixture onto a stainless-steel 384-well target (BrukerDaltonics, Germany). In negative-ion and reflectron mode, each final mass spectrum was accumulated as an average of 5000 single-shot spectra. Laser fluence was set to 72 $\mu J/100\ \mu m^2$.

Synthesis of Polyadenosine-Stabilized AuNCs. A 500 μL volume of aqueous solution containing $HAuCl_4$ (1 mM, 10−100 μL), polyadenosine, (A10-A50; 10 μM, 50 μL), and sodium citrate (pH 6; 100 mM, 25 μL) was prepared in a quartz cuvette at ambient temperature. Parafilm was used to seal the containers. The as-prepared solution was exposed to UV-emitting LED (UVTOP295, Roithner Laser Technik, Vienna, Austria; λ_{max} = 305 nm; optical power = 500 μW at 20 mA) in a dark box at ambient temperature for 0−36 h (Figure S24). The concentration of the as-synthesized AuNCs was denoted as 1× in this study. To test the effect of the wavelength on the photoassisted synthesis of AuNCs, this study replaced UV LED with a green-emitting LED (λ_{max} = 525 nm; optical power = 180 mW) and a red-emitting LED (λ_{max} = 635 nm; optical power = 180 mW). Additionally, other buffer systems, including sodium acetate, sodium phosphate, and Tris-HCl, were used in place of sodium citrate. To develop ratiometric probe, ssDNA (5′-A_{30} CAT CAT AGT CCA GTG TCC AGG G-3′) was used to synthesize AuNCs under the same conditions as provided in the preparation of A_{30}-stabilized AuNCs. The concentration of AuNC-bearing ssDNA was denoted as 1× in this study.

Sensing of Target DNA. All samples were prepared in 10 mM Tris-HCl at pH 7.0. Different concentrations of DNA_{pm} (0−1 μM, 200 μL; 5′-CCC TGG ACA CTG GAC TAT GAT G-3′) was mixed with A_{30}-stabilized AuNCs (1× , 40 μL) at 40 °C for 30 min. A solution of SG (250 nM, 160 μL) was incubated with the resulting solution at ambient temperature for another 30 min. The resulting solutions were transferred into a 1 mL quartz cuvette. Their fluorescence spectra were recorded by operating the fluorescence spectrophotometer at an excitation wavelength of 290 nm. The selectivity of A_{30}-stabilized AuNCs was tested by replacing DNA_{pm} one at a time with single-base-mismatched DNA (5′-CCC TGG GCA CTG GAC TAT GAT G-3′), double-base-mismatched DNA (5′-CCC TGG GCA CTG GAC TCT GAT G-3′), and nontarget DNA (5′-TTC CCA CCC ACC CCG GCC C GT T-3′).

To quantify DNA_{pm} in real samples, blood samples were collected from a healthy adult male (age = 24 years). The whole blood samples were immediately centrifuged at 10 000 rpm for 10 min. The obtained plasma samples (100 μL) were spiked with standard solutions of DNA_{pm} (0−400 nM, 100 μL). The spiked samples were treated with the PureLink Genomic DNA Mini Kit (200 μL; Life Technologies). The purified samples (40 μL) were incubated with a solution containing AuNC-bearing ssDNA (1× , 40 μL), SG (1 μM, 40 μL), and 20 mM Tris-HCl (1 μM, 280 μL) at ambient temperature for 30 min.

ASSOCIATED CONTENT

Supporting Information

The Supporting Information is available free of charge on the ACS Publications website at DOI: 10.1021/acsami.5b07766.

Fluorescence, emission, and absorbance spectra, including those recorded under varying conditions of pH, storage, and UV exposure, synthesis validation data, size-exclusion chromatograms, mass spectra, TEM images, cyclic voltammogram, ratiometric sensing data, and schematic of sysnthesis process as described in text. (PDF)

DOI: 10.1021/acsami.5b07766
ACS Appl. Mater. Interfaces 2015, 7, 23708−23716

AUTHOR INFORMATION

Corresponding Author

*E-mail: tsengwl@mail.nsysu.edu.tw. Phone: 011-886- 7-5254644. Fax: 011-886-7-3684046.

Notes

The authors declare no competing financial interest.

ACKNOWLEDGMENTS

We thank the Ministry of Science and Technology (NSC 100-2628-M-110-001- MY4) for the financial support of this study.

REFERENCES

(1) Jain, P. K.; Huang, X.; El-Sayed, I. H.; El-Sayed, M. A. Noble Metals on the Nanoscale: Optical and Photothermal Properties and Some Applications in Imaging, Sensing, Biology, and Medicine. *Acc. Chem. Res.* **2008**, *41* (12), 1578−1586.

(2) Daniel, M.-C.; Astruc, D. Gold Nanoparticles: Assembly, Supramolecular Chemistry, Quantum-Size-Related Properties, and Applications toward Biology, Catalysis, and Nanotechnology. *Chem. Rev.* **2004**, *104* (1), 293−346.

(3) Zheng, J.; Nicovich, P. R.; Dickson, R. M. Highly Fluorescent Noble-Metal Quantum Dots. *Annu. Rev. Phys. Chem.* **2007**, *58*, 409−431.

(4) Chen, S.; Ingram, R. S.; Hostetler, M. J.; Pietron, J. J.; Murray, R. W.; Schaaff, T. G.; Khoury, J. T.; Alvarez, M. M.; Whetten, R. L. Gold Nanoelectrodes of Varied Size: Transition to Molecule-Like Charging. *Science* **1998**, *280* (5372), 2098−2101.

(5) Laaksonen, T.; Ruiz, V.; Liljeroth, P.; Quinn, B. M. Quantised Charging of Monolayer-Protected Nanoparticles. *Chem. Soc. Rev.* **2008**, *37* (9), 1836−1846.

(6) Chen, L.-Y.; Wang, C.-W.; Yuan, Z.; Chang, H.-T. Fluorescent Gold Nanoclusters: Recent Advances in Sensing and Imaging. *Anal. Chem.* **2015**, *87* (1), 216−229.

(7) Tao, Y.; Lin, Y. H.; Huang, Z. Z.; Ren, J. S.; Qu, X. G. Incorporating Graphene Oxide and Gold Nanoclusters: A Synergistic Catalyst with Surprisingly High Peroxidase-Like Activity Over a Broad pH Range and its Application for Cancer Cell Detection. *Adv. Mater.* **2013**, *25* (18), 2594−2599.

(8) Ju, E. G.; Liu, Z.; Du, Y. D.; Tao, Y.; Ren, J. S.; Qu, X. G. Heterogeneous Assembled Nanocomplexes for Ratiometric Detection of Highly Reactive Oxygen Species in Vitro and in Vivo. *ACS Nano* **2014**, *8* (6), 6014−6023.

(9) Chen, Y.; Yang, T.; Pan, H.; Yuan, Y.; Chen, L.; Liu, M.; Zhang, K.; Zhang, S.; Wu, P.; Xu, J. Photoemission Mechanism of Water-Soluble Silver Nanoclusters: Ligand-to-Metal−Metal Charge Transfer vs Strong Coupling between Surface Plasmon and Emitters. *J. Am. Chem. Soc.* **2014**, *136* (5), 1686−1689.

(10) Desireddy, A.; Conn, B. E.; Guo, J.; Yoon, B.; Barnett, R. N.; Monahan, B. M.; Kirschbaum, K.; Griffith, W. P.; Whetten, R. L.; Landman, U.; Bigioni, T. P. Ultrastable silver nanoparticles. *Nature* **2013**, *501* (7467), 399−402.

(11) Wang, T.; Hu, X.; Dong, S. The Fragmentation of Gold Nanoparticles Induced by Small Biomolecules. *Chem. Commun.* **2008**, *38*, 4625−4627.

(12) Xu, Y.; Sherwood, J.; Qin, Y.; Crowley, D.; Bonizzoni, M.; Bao, Y. The Role of Protein Characteristics in the Formation and Fluorescence of Au Nanoclusters. *Nanoscale* **2014**, *6* (3), 1515−1524.

(13) Huang, C.-C.; Yang, Z.; Lee, K.-H.; Chang, H.-T. Synthesis of Highly Fluorescent Gold Nanoparticles for Sensing Mercury(II). *Angew. Chem., Int. Ed.* **2007**, *46* (36), 6824−6828.

(14) Lin, C.-A. J.; Yang, T.-Y.; Lee, C.-H.; Huang, S. H.; Sperling, R. A.; Zanella, M.; Li, J. K.; Shen, J.-L.; Wang, H.-H.; Yeh, H.-I.; Parak, W. J.; Chang, W. H. Synthesis, Characterization, and Bioconjugation of Fluorescent Gold Nanoclusters toward Biological Labeling Applications. *ACS Nano* **2009**, *3* (2), 395−401.

(15) Huang, C.-C.; Chen, C.-T.; Shiang, Y.-C.; Lin, Z.-H.; Chang, H.-T. Synthesis of Fluorescent Carbohydrate-Protected Au Nanodots for Detection of Concanavalin A and Escherichia coli. *Anal. Chem.* **2009**, *81* (3), 875−882.

(16) Habeeb Muhammed, M.; Ramesh, S.; Sinha, S.; Pal, S.; Pradeep, T. Two Distinct Fluorescent Quantum Clusters of Gold Starting from Metallic Nanoparticles by pH-Dependent Ligand Etching. *Nano Res.* **2008**, *1* (4), 333−340.

(17) Shang, L.; Yang, L.; Stockmar, F.; Popescu, R.; Trouillet, V.; Bruns, M.; Gerthsen, D.; Nienhaus, G. U. Microwave-Assisted Rapid Synthesis of Luminescent Gold Nanoclusters for Sensing Hg^{2+} in Living Cells Using Fluorescence Imaging. *Nanoscale* **2012**, *4* (14), 4155−4160.

(18) Shang, L.; Stockmar, F.; Azadfar, N.; Nienhaus, G. U. Intracellular Thermometry by Using Fluorescent Gold Nanoclusters. *Angew. Chem., Int. Ed.* **2013**, *52* (42), 11154−11157.

(19) Wang, Z.; Cai, W.; Sui, J. Blue Luminescence Emitted from Monodisperse Thiolate-Capped Au11 Clusters. *ChemPhysChem* **2009**, *10* (12), 2012−2015.

(20) Zheng, J.; Petty, J. T.; Dickson, R. M. High Quantum Yield Blue Emission from Water-Soluble Au8 Nanodots. *J. Am. Chem. Soc.* **2003**, *125* (26), 7780−7781.

(21) Xie, J.; Zheng, Y.; Ying, J. Y. Protein-Directed Synthesis of Highly Fluorescent Gold Nanoclusters. *J. Am. Chem. Soc.* **2009**, *131* (3), 888−889.

(22) Kennedy, T. A. C.; MacLean, J. L.; Liu, J. Blue Emitting Gold Nanoclusters Templated by Poly-cytosine DNA at Low pH and Poly-adenine DNA at Neutral pH. *Chem. Commun.* **2012**, *48* (54), 6845−6847.

(23) Liu, G.; Shao, Y.; Ma, K.; Cui, Q.; Wu, F.; Xu, S. Synthesis of DNA-templated fluorescent gold nanoclusters. *Gold Bull.* **2012**, *45* (2), 69−74.

(24) Lopez, A.; Liu, J. W. Light-Activated Metal-Coordinated Supramolecular Complexes with Charge-Directed Self-Assembly. *J. Phys. Chem. C* **2013**, *117* (7), 3653−3661.

(25) McGilvray, K. L.; Decan, M. R.; Wang, D.; Scaiano, J. C. Facile Photochemical Synthesis of Unprotected Aqueous Gold Nanoparticles. *J. Am. Chem. Soc.* **2006**, *128* (50), 15980−15981.

(26) Torigoe, K.; Esumi, K. Preparation of Colloidal Gold by Photoreduction of Tetracyanoaurate(1-)-Cationic Surfactant Complexes. *Langmuir* **1992**, *8* (1), 59−63.

(27) Carbone, L.; Jakab, A.; Khalavka, Y.; Sönnichsen, C. Light-Controlled One-Sided Growth of Large Plasmonic Gold Domains on Quantum Rods Observed on the Single Particle Level. *Nano Lett.* **2009**, *9* (11), 3710−3714.

(28) Quintana, M.; Ke, X.; Van Tendeloo, G.; Meneghetti, M.; Bittencourt, C.; Prato, M. Light-Induced Selective Deposition of Au Nanoparticles on Single-Wall Carbon Nanotubes. *ACS Nano* **2010**, *4* (10), 6105−6113.

(29) Chen, Y.-M.; Yu, C.-J.; Cheng, T.-L.; Tseng, W.-L. Colorimetric Detection of Lysozyme Based on Electrostatic Interaction with Human Serum Albumin-Modified Gold Nanoparticles. *Langmuir* **2008**, *24* (7), 3654−3660.

(30) Park, J.-W.; Shumaker-Parry, J. S. Structural Study of Citrate Layers on Gold Nanoparticles: Role of Intermolecular Interactions in Stabilizing Nanoparticles. *J. Am. Chem. Soc.* **2014**, *136* (5), 1907−1921.

(31) Wu, X.; Redmond, P. L.; Liu, H.; Chen, Y.; Steigerwald, M.; Brus, L. Photovoltage Mechanism for Room Light Conversion of Citrate Stabilized Silver Nanocrystal Seeds to Large Nanoprisms. *J. Am. Chem. Soc.* **2008**, *130* (29), 9500−9506.

(32) Xue, C.; Métraux, G. S.; Millstone, J. E.; Mirkin, C. A. Mechanistic Study of Photomediated Triangular Silver Nanoprism Growth. *J. Am. Chem. Soc.* **2008**, *130* (26), 8337−8344.

(33) Zheng, J.; Nicovich, P. R.; Dickson, R. M. Highly Fluorescent Noble-Metal Quantum Dots. *Annu. Rev. Phys. Chem.* **2007**, *58* (1), 409−431.

(34) Chen, T.-H.; Tseng, W.-L. (Lysozyme Type VI)-Stabilized Au8 Clusters: Synthesis Mechanism and Application for Sensing of Glutathione in a Single Drop of Blood. *Small* **2012**, *8* (12), 1912−1919.

DOI: 10.1021/acsami.5b07766
ACS Appl. Mater. Interfaces 2015, 7, 23708−23716

(35) Le Guével, X.; Hötzer, B.; Jung, G.; Hollemeyer, K.; Trouillet, V.; Schneider, M. Formation of Fluorescent Metal (Au, Ag) Nanoclusters Capped in Bovine Serum Albumin Followed by Fluorescence and Spectroscopy. *J. Phys. Chem. C* **2011**, *115* (22), 10955−10963.
(36) Duan, H.; Nie, S. Etching Colloidal Gold Nanocrystals with Hyperbranched and Multivalent Polymers: A New Route to Fluorescent and Water-Soluble Atomic Clusters. *J. Am. Chem. Soc.* **2007**, *129* (9), 2412−2413.
(37) Bao, Y.; Zhong, C.; Vu, D. M.; Temirov, J. P.; Dyer, R. B.; Martinez, J. S. Nanoparticle-Free Synthesis of Fluorescent Gold Nanoclusters at Physiological Temperature. *J. Phys. Chem. C* **2007**, *111* (33), 12194−12198.
(38) Lan, G. Y.; Chen, W. Y.; Chang, H. T. One-Pot Synthesis of Fluorescent Oligonucleotide Ag Nanoclusters for Specific and Sensitive Detection of DNA. *Biosens. Bioelectron.* **2011**, *26* (5), 2431−2435.
(39) Sharma, J.; Yeh, H. C.; Yoo, H.; Werner, J. H.; Martinez, J. S. A Complementary Palette of Fluorescent Silver Nanoclusters. *Chem. Commun.* **2010**, *46* (19), 3280−3282.
(40) Obliosca, J. M.; Babin, M. C.; Liu, C.; Liu, Y.-L.; Chen, Y.-A.; Batson, R. A.; Ganguly, M.; Petty, J. T.; Yeh, H.-C. A Complementary Palette of NanoCluster Beacons. *ACS Nano* **2014**, *8* (10), 10150−10160.
(41) Fu, Y.; Xu, S.; Pan, C.; Ye, M.; Zou, H.; Guo, B. A Matrix of 3,4-diaminobenzophenone for the Analysis of Oligonucleotides by Matrix-Assisted Laser Desorption/Ionization Time-of-Flight Mass Spectrometry. *Nucleic Acids Res.* **2006**, *34* (13), e94.
(42) Abdi, F.; Bradbury, E. M.; Doggett, N.; Chen, X. Rapid Characterization of DNA Oligomers and Genotyping of Single Nucleotide Polymorphism Using Nucleotide-Specific Mass Tags. *Nucleic Acids Res.* **2001**, *29* (13), e61.
(43) Lopez, A.; Liu, J. W. DNA-Templated Fluorescent Gold Nanoclusters Reduced by Good's Buffer: from Blue-Emitting Seeds to Red and Near Infrared Emitters. *Can. J. Chem.* **2015**, *93* (6), 615−620.
(44) Minaga, T.; Kun, E. Spectral Analysis of the Conformation of Polyadenosine Diphosphoribose. Evidence Indicating Secondary Structure. *J. Biol. Chem.* **1983**, *258* (2), 725−730.
(45) Grzelczak, M.; Liz-Marzan, L. M. The Relevance of Light in the Formation of Colloidal Metal Nanoparticles. *Chem. Soc. Rev.* **2014**, *43* (7), 2089−2097.
(46) Zhu, S.; Gorski, W.; Powell, D. R.; Walmsley, J. A. Synthesis, Structures, and Electrochemistry of Gold(III) Ethylenediamine Complexes and Interactions with Guanosine 5′-Monophosphate. *Inorg. Chem.* **2006**, *45* (6), 2688−2694.
(47) Chen, H.-H.; Huang, J.-F. EDTA Assisted Highly Selective Detection of As^{3+} on Au Nanoparticle Modified Glassy Carbon Electrodes: Facile in Situ Electrochemical Characterization of Au Nanoparticles. *Anal. Chem.* **2014**, *86* (24), 12406−12413.
(48) Obliosca, J. M.; Liu, C.; Yeh, H.-C. Fluorescent Silver Nanoclusters as DNA Probes. *Nanoscale* **2013**, *5* (18), 8443−8461.
(49) Pei, H.; Li, F.; Wan, Y.; Wei, M.; Liu, H.; Su, Y.; Chen, N.; Huang, Q.; Fan, C. Designed Diblock Oligonucleotide for the Synthesis of Spatially Isolated and Highly Hybridizable Functionalization of DNA−Gold Nanoparticle Nanoconjugates. *J. Am. Chem. Soc.* **2012**, *134* (29), 11876−11879.
(50) Pyykko, P. Structural Properties: Magic Nanoclusters of Gold. *Nat. Nanotechnol.* **2007**, *2* (5), 273−274.
(51) Zhou, L.; Wang, Q.; Zhang, X.-B.; Tan, W. Through-Bond Energy Transfer-Based Ratiometric Two-Photon Probe for Fluorescent Imaging of Pd^{2+} Ions in Living Cells and Tissues. *Anal. Chem.* **2015**, *87* (8), 4503−4507.
(52) Jockusch, S.; Martí, A. A.; Turro, N. J.; Li, Z.; Li, X.; Ju, J.; Stevens, N.; Akins, D. L. Spectroscopic Investigation of a FRET Molecular Beacon Containing Two Fluorophores for Probing DNA/RNA Sequences. *Photochem. Photobiol. Sci.* **2006**, *5* (5), 493−498.
(53) Zhang, P.; Beck, T.; Tan, W. Design of a Molecular Beacon DNA Probe with Two Fluorophores. *Angew. Chem., Int. Ed.* **2001**, *40* (2), 402−405.
(54) Richards, C. I.; Choi, S.; Hsiang, J. C.; Antoku, Y.; Vosch, T.; Bongiorno, A.; Tzeng, Y. L.; Dickson, R. M. Oligonucleotide-Stabilized Ag Nanocluster Fluorophores. *J. Am. Chem. Soc.* **2008**, *130* (15), 5038−5039.

DOI: 10.1021/acsami.5b07766
ACS Appl. Mater. Interfaces 2015, 7, 23708−23716